The Effect of Conductor Processing and Properties on Additively Manufactured Antenna Performance.

Emuobosan Enakerakpo, Waleed Tawfik Al-Shaibani, Olya Noruz Shamsian, Riadh Al-Haidari, Abdullah Obeidat S., Ashraf Umar, Mohammed Alhendi, Mark Poliks.
The Center for Advanced Microelectronics Manufacturing (CAMM), State University of New York at Binghamton, Binghamton, NY, 13902 USA
Email: eenaker1@binghamton.edu

Abstract

Printed electronics techniques are increasingly utilized for device fabrication, particularly in flexible electronics. This study investigates the performance trade-offs associated with additive printed electronics methods and materials, focusing on antenna gain. A dual-band dipole antenna, operating at 2.4 GHz and 4.6 GHz, was designed using the ANSYS High-Frequency Structure Simulator (HFSS), with printed silver as the conductive material and 5mil (125 µm) Kapton as the substrate. Three sets of antennas, each with different conductive materials and printing techniques, were fabricated while maintaining a consistent substrate and antenna design. The fabrication techniques include dispensing and aerosol jet printing, with the conductive materials varying in particle size. Results show that resistance primarily affects antenna gain at 2.4 GHz, while the microstructure of the conductive material plays a more significant role at 4.6 GHz.

Key words
Printed Electronics, Antenna, Dipole, Antenna gain, Aerosol Jet Printing, Precision Dispensing.

I. Introduction

With the proliferation of the internet of things, and wearable devices that require technology like antennas on package, there is increased demand for components to meet the SWaP requirements. Antennas are one of the device components to facilitate the development[1]–[4]. Aside from the SWaP requirements, fabrication cost and material processing seem to be other constraints in the conventional fabrication of these components onto the device substrate without needing any form of transfer. This is where AM bridges offer advantages by offering processes having low thermal requirements, low material waste while facilitating complex designs quickly[5][6].

The development of novel materials in the form of electrically functional inks or paste has enabled additive manufacturing (AM) techniques, an alternative to conventional methods, to be utilized in the fabrication of electronic devices. Additive manufacturing offers numerous advantages, including cost savings, waste reduction, design flexibility, and rapid prototyping. Despite the many advantages of AM as an alternative or rival to established processes, there are still gaps in the literature that provide information on the potential trade-offs in the functionality of devices fabricated using AM techniques. More information is therefore required to compare the performance of various printed conductive materials fabricated with different printing techniques.

Many studies to understand the effect of material on conductivity rely mostly on simulation which makes it difficult to integrate the effects of the microstructure. For example, Shahpari and David did show numerically the effect of conductivity on antenna gain where thy concluded that the dipole gain G is only affected by conductivity $<5x10^5$S/m. this was however different for a Yagi or Meander which are affected by variations in only in considerably lower conductivities [7]. Mohammed et al. studied the effect of conductor, substrate and ground thickness on the gain of a patch antenna designed for 28GHz using numeric analysis [8]. Gaozhi et al. reported an increase in the Q-factor of a high frequency loop antenna intended for RFID application after densifying the microstructure by thermal compression or near infrared (NIR) annealing treatment[9]. In another case the The thickness of printed antenna conductors has been shown to be proportional to the gain of an antenna, however, the effect of the structure thickness may be negligible beyond two times the skin depth (δ) [10]

In this work, we study the effects of conductor properties and processing, resistivity and dimensions on antenna gain. To this end, we designed a dual-band dipole antenna operating at 2.4 GHz and 4.6 GHz —which we termed Low and High frequency respectively—using the ANSYS High-Frequency Structure Simulator (HFSS). All samples were fabricated on a 5 mil (125µm) Kapton HN from Dupont. To ensure a fair comparison, we fabricated three sets of antennas, using different conductive materials and fabrication techniques, while keeping the substrate and antenna design consistent. These printing techniques included dispensing and aerosol jet printing which are both direct write techniques but differ in the deposition technique, print resolution and the structure profile. Dispensing deposit pastes with very high silver loading, while aerosol jet printing deposits ink with much less solid loading.

II. Design and material.

In this work we designed a dual band dipole antenna with dimensions identical to the antenna design in [3]with target frequency of 2.4GHz and 4.6GHz and simulated the design using the ANSYS HFSS. In the designed antenna, arm A of the antenna is the high frequency arm (5GHz) while arm B is the low frequency (2.4GHz) arm (Fig. 1).

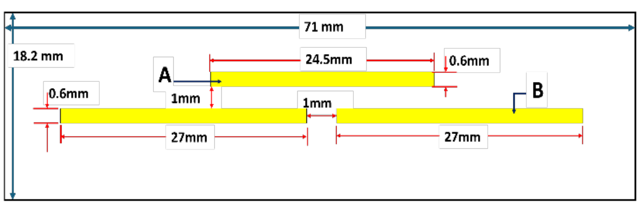

Fig. 1 Antenna design showing dimensions of dipole and the coupled antenna. A is the high frequency arm and B is the low frequency arm

The substrate is 5mil Dupont Kapton HN with a dielectric constant (dk) of 3.5 and a dissipation factor (df) of 0.0026 which has acceptable dimensional stability at temperatures up to 200°C and CTE of 16ppm/°C [11]. The conductor in the simulation is bulk copper with a conductivity of 5.8e7 S/m.

III. Fabrication

In this work we fabricated with (i) the aerosol jet printing method described in [12], [13] which is suitable for inks with viscosities ranging from 1cp to 1500cp and useful for printing high-resolution, low-profile structures and (ii) precision dispense[14] which is more suited for printing paste with higher viscosities therefore allowing materials with higher solid loading. It is worth noting that the dispensing printing process is considerably faster than the printing while the AJP offers higher resolution of printed structures. The Aerosol Jet printer is an Optomec 3-axis sprint printer while the dispensed printer is Nordson EFD. Table 1 shows the summary of the printed conductor properties and the processing conditions.

The conductive materials were (i) Novacentrix HPS-108AE1 Silver Nanoflakes ink, a water-based ink having 60wt% Ag loading, (ii) Dupont 5025 with silver micro flakes particles and (iii) a silver-based ink from ACI materials Inc., which has a semi sintered mixture of micro flakes and nano spherical particles for increase conductivity. After printing, samples were processed at manufacturers recommended temperature which are highlighted in Table 1. Thereafter, coaxial RF SMA connectors were attached with a conductive adhesive, Nagase ChemteX, CA-188-2 which was cured in oven at 80°C for 1 hour.

Table 1 Summary of conductor properties and processing conditions and processability.

	Dupont	ACI	Novacentrix
Fabrication process	Precision Dispense	Precision Dispense	Aerosol jet printing
Sintering Profile	120°C/15mins	120°C/10mins	200C/1 hr
Particle type	micro flakes	Micro flakes and microparticles	Micro flakes
Thickness (µm)	11.758 ± 2.678	21.42 ± 12.36	6.40 ± 0.445
Width (µm)	567 ± 30.5	596 ± 15.49	605 ± 3.34
Resistivity (Ω.mm/sq)	3.41E-4 ± 5.01E-5	1.76E-4 ± 4.53E-5	2.57E-4 ± 2.65E-5

IV. Measurements and Testing

The physical dimensions of the fabricated structures were obtained and analyzed with a confocal laser microscope (Keyence VK-X1050 series) at 10X magnification. A digital multimeter (Keithley 2100) was used to obtain two-point DC resistance measurement from the entire length of the coupled antenna (part A) in Fig. 1 to obtain the sheet resistivity of the conductor on the substrate. A vector Network Analyzer (VNA), ZNB 40 by Rhodes and Swartz rated up to 40GHz was used to obtain the RF parameters and in combination with an anechoic chamber which is equipped with a 18GHz Quad Ridge Horn Antenna from "The EMCShop" (model: QRHA18G-OB) was used to obtain the antenna gain. The antenna gain was obtained using the Diamond Engineering

Antenna Measurement Studio which uses the Friis free space equation given below [15].

$$P_r = \left(\frac{\lambda}{4\pi d}\right)^2 G_t G_r G_p \quad (1)$$

$$G_r = \left(\frac{4\pi d}{\lambda}\right)^2 \left(\frac{P_r}{P_t}\right) G_t \quad (2)$$

$$\left(\frac{P_r}{P_t}\right) = (S_{21})^2 \quad (3)$$

Where P_r is received antenna power and P_t is transmitted power, G_r is received antenna gain while G_t is transmitted antenna gain, d is the distance between the receiving antenna and the transmitting antenna and λ is the wavelength for the frequency of interest.

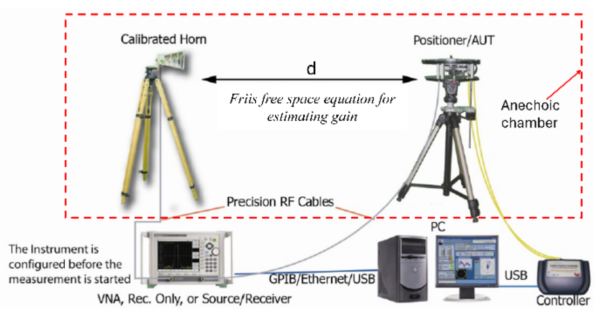

Fig. 2 Antenna gain measurement set up.

For the analysis, four samples were taken for each of the three material types making a total of 12 samples. Minitab was used to run all statistical analysis.

V. Results and discussion

Fig. 3 illustrates the impact of fabrication method and material on the profile and dimensions of the printed structures. As expected, the aerosol jet (AJ) printed structures are thinner, measuring around 6 µm, compared to the dispensed structures using DP5025 and ACI materials, which have thicknesses of 12 µm and 20 µm, respectively. The AJ printed structures also exhibit minimal variability in thickness compared to the dispensed structures. In contrast, the ACI structures show significant thickness variability due to the tackiness of the material, which also leads to a non-uniform profile shape, as shown in Fig. 4. The AJ printing process produces a ridged profile because of the rastering tool path used to fill the conductor area and the rapid drying during printing. Among the three methods, the DP5025 material and process result in the most uniform profile in terms of roughness and overall form.

Also, in Fig. 3b we see the effects of processing and material on the final width of the printed structures. the aerosol jet printing process is seen to be much closer to the target width of 600µm with minimal variability. This is due to the high resolution of the printing process which results from the small volume of aerosol droplets formed. This makes it more suited for fabricating components or devices requiring a target planar dimension such as high frequency antenna as these are easily achievable within a small margin of variation.

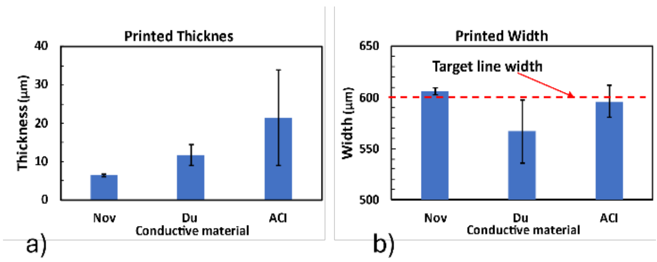

Fig. 3 Effect of materials and processing on Profile structure. a) Effect on thickness and, b) effect on width.

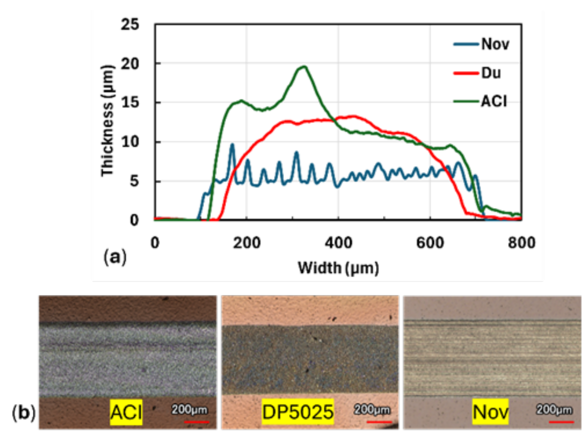

Fig. 4 Profile of printed structures obtained from the high frequency arm. (a) Profile of printed structures and (b) optical image of printed structures.

Fig. 5 shows the SEM images of the printed and sintered inks, revealing the microstructure of the Novacentrix and Dupont materials after sintering. However, the microstructure of the ACI material is not displayed due to proprietary concerns. The Novacentrix particles are less than 1 µm in size and have a large aspect ratio, while the Dupont 5025 particles are around 5 µm with a smaller aspect ratio. The ACI material, which contains a few spherical particles, also features flakes approximately 3 µm in size with aspect ratios larger than those of the Novacentrix ink, owing to their similar thickness.

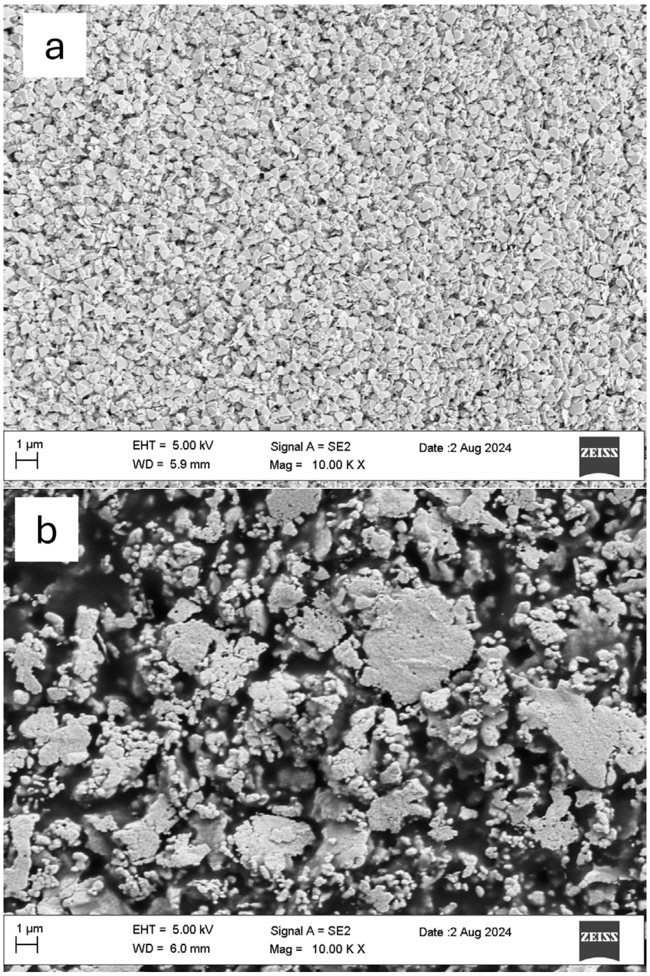

Fig. 5 Microstructure of processed materials obtained using a Zeiss FE-SEM Supra-55 VP (a)Novacentrix with magnification at 20Kx and (b) Dupont 5025 with magnification at 3Kx.

The resistivity of the printed structures shows the DP5025 having the highest average sheet resistivity of 0.34 mΩ.mm/sq, which is almost two times the sheet resistivity of the ACI at 0.176 mΩ.mm/sq (Table 1). The resistance of the final structures is highest for the Novacentrix due to the comparatively low-profile thickness even with an average sheet resistivity of 0.274 mΩ.mm/sq. Fig. 6 also show the effect of aging at 85°C/85%RH conditions. Results indicate identical reduction in the resistance and resistivity of structures of all material types to around 84% of the initial value. Samples were further dried at 100°C to remove the effect of moisture on the resistivity. Resistivity after drying showed that the possible presence of moisture had negligible effect on the resistivity. Possible reasons could be attributed to the change in the microstructure which have been weathered down due to the aging process[16].

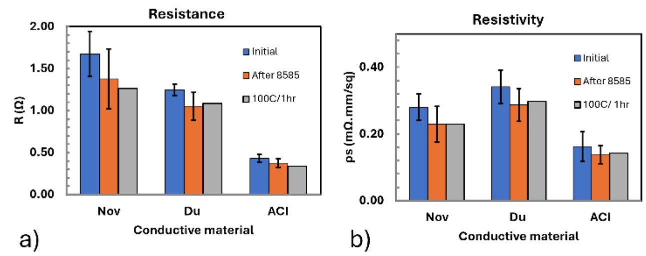

Fig. 6 DC characterization of printed structures. a) Resistivity of printed conductor and, b) resistance of part A of antenna.

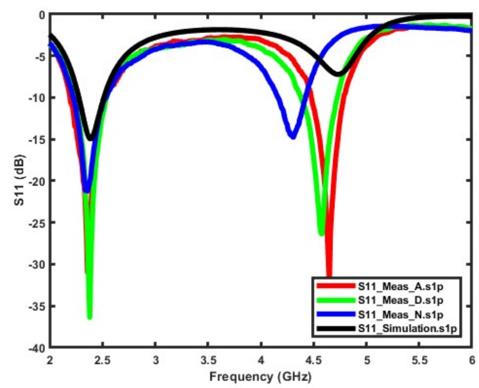

Fig. 7 Antenna return loss measurements.

Fig. 7 shows that all conductor materials for the fabricated antennas share the same overlapping low resonance frequency. However, their high frequencies differ, with Novacentrix having the lowest resonance frequency, followed by Dupont, and then ACI. All these resonance frequencies are lower than the simulated predictions, a pattern also noted in [17], where antenna length adjustments were necessary to keep the target frequency within the desired design bandwidth. This frequency shift is likely due to the binding material in the printed conductor and at the interface with the substrate, which is not accounted for in simulations and may change the substrate's effective dielectric properties.

In this work we have considered the microstructure to be a result of the material type and processing conditions. Fig. 8 illustrates the impact of material and processing on the maximum antenna gain at both low and high frequencies. At the low frequency, the ACI material achieves the highest gain, followed by DP5025, while at the high frequency, Novacentrix provides the highest maximum gain, followed by ACI. The maximum gain occurs when the elevation is at 0° across all azimuth angles from 0° to 360°.

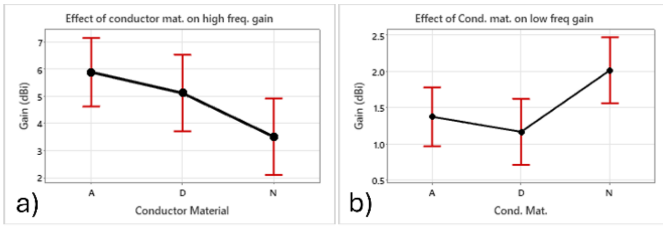

Fig. 8 Effect of Processing and material on antenna gain. a) High frequency gain and, b) Low frequency gain.

A regression analysis was conducted to determine which parameter of the antenna is the primary predictor of higher gain, using material-and-process for microstructure representation, resistivity (ρ), resistance (R), thickness (T), and width (W) as independent variables. The results indicate that resistance, with a low p-value, is the most significant predictor of antenna gain at the low frequency of 2.4 GHz, while resistivity is the least significant factor.

For the high frequency, the initial analysis showed the width to be the least important. Further analysis was conducted with the width removed. This showed the material-and-process to be the most significant factor with the resistance following close in significance.

The microstructure made up of smaller particle size on average offered the highest gain at the high frequency being from nano-flakes in comparison to the dispensed materials made up of micro-flakes. The aging of the samples at 85C/85RH resulted in marginal increase in the antenna gain at the high frequency band Fig. 9. The increase in gain may be explained by the likely break down of the microstructure into finer particle as seen in [16]. The gain of the low frequency band after aging had a random behavior and this may be due to damage in the bond material been the SMA connector and the antenna which is bonded at the low frequency arm. Fig. 10 shows a completely fabricated antenna.

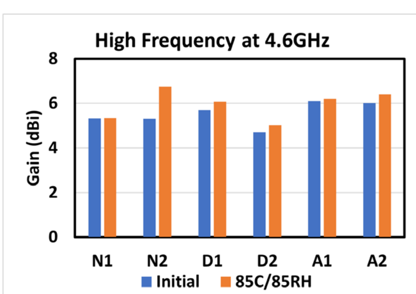

Fig. 9 Effect of aging on the gain at the high frequency.

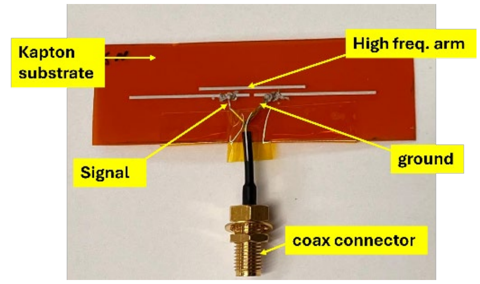

Fig. 10 Complete fabricated dipole antenna

VI. Conclusion

In this study, a dual-band dipole antenna, designed to operate at 2.4 GHz and 4.6 GHz, was fabricated on Kapton HN using three different ink materials. The physical and electrical properties of the antenna were analyzed to assess their impact on antenna gain. The results showed that at low frequencies, gain was more influenced by the resistance, with lower resistance leading to higher gain. At high frequencies, gain was more affected by the microstructure of the material, where a finer microstructure resulted in better performance. These findings highlight the critical role of the internal microstructure of conductors in high-frequency applications, as printed electronics become more widely used.

References

[1] W. Yang, X. Cheng, Z. Guo, Q. Sun, J. Wang, and C. Wang, “Design, fabrication and applications of flexible RFID antennas based on printed electronic materials and technologies,” *J. Mater. Chem. C*, vol. 11, no. 2, pp. 406–425, Jan. 2023, doi: 10.1039/D2TC03736J.

[2] C. Wang *et al.*, “New Advances in Antenna Design toward Wearable Devices Based on Nanomaterials,” *Biosensors*, vol. 14, no. 1, p. 35, Jan. 2024, doi: 10.3390/bios14010035.

[3] E. Enakerakpo *et al.*, “Performance of Flexible Microwave Antenna Under Environmental Stress,” in *2022 IEEE 72nd Electronic Components and Technology Conference (ECTC)*, May 2022, pp. 1927–1933, doi: 10.1109/ECTC51906.2022.00302.

[4] T.-H. Lin, R. Bahr, M. M. Tentzeris, P. M. Raj, V. Sundaram, and R. Tummala, “Novel 3D-/Inkjet-Printed Flexible On-package Antennas, Packaging Structures, and Modules for Broadband 5G Applications,” in *2018 IEEE 68th Electronic Components and Technology Conference (ECTC)*, May 2018, pp. 214–220, doi:

10.1109/ECTC.2018.00041.

[5] A. S. Obeidat *et al.*, “Embedded RF Packaging Via Ceramic 3D Printing and Printed Electronics Additive Manufacturing,” in *2024 IEEE 74th Electronic Components and Technology Conference (ECTC)*, May 2024, pp. 685–692, doi: 10.1109/ECTC51529.2024.00112.

[6] S. Lieberman *et al.*, “Electrical Behavior of Thin Die Assembly on Flexible Substrate Under Vibration Testing,” in *2024 IEEE 74th Electronic Components and Technology Conference (ECTC)*, May 2024, pp. 1670–1676, doi: 10.1109/ECTC51529.2024.00276.

[7] M. Shahpari and D. V. Thiel, “The Impact of Reduced Conductivity on the Performance of Wire Antennas,” *IEEE Trans. Antennas Propag.*, vol. 63, no. 11, pp. 4686–4692, Nov. 2015, doi: 10.1109/TAP.2015.2479241.

[8] A. S. Mohammed *et al.*, “Improving the Gain Performance of Air Substrate Patch Antenna Array Using the Effect of Conductive Material Thickness Study for 5G Applications,” *J. Phys. Conf. Ser.*, vol. 1529, no. 5, p. 052020, May 2020, doi: 10.1088/1742-6596/1529/5/052020.

[9] G. Xiao, Z. Zhang, H. Fukutani, Y. Tao, and S. Lang, “Improving the Q-Factor of Printed HF RFID Loop Antennas on Flexible Substrates by Condensing the Microstructures of Conductors,” *IEEE J. Radio Freq. Identif.*, vol. 2, no. 2, pp. 111–116, Jun. 2018, doi: 10.1109/JRFID.2018.2854264.

[10] S. L. Merilampi, T. Bjorninen, A. Vuorimaki, L. Ukkonen, P. Ruuskanen, and L. Sydanheimo, “The Effect of Conductive Ink Layer Thickness on the Functioning of Printed UHF RFID Antennas,” *Proc. IEEE*, vol. 98, no. 9, pp. 1610–1619, Sep. 2010, doi: 10.1109/JPROC.2010.2050570.

[11] A. S. Obeidat *et al.*, “Effect of Thermal and Mechanical Stresses on Novel Microstrip Lines Printed on Flexible Substrates,” *IEEE Trans. Components, Packag. Manuf. Technol.*, vol. 14, no. 8, pp. 1481–1492, Aug. 2024, doi: 10.1109/TCPMT.2024.3412740.

[12] E. Enakerakpo *et al.*, “Fully Additive Manufacturing of Passive Circuit Elements using Aerosol Jet Printing,” in *2021 IEEE 71st Electronic Components and Technology Conference (ECTC)*, Jun. 2021, pp. 1138–1143, doi: 10.1109/ECTC32696.2021.00186.

[13] R. Ross Salary, J. P. Lombardi III, D. L. Weerawarne, P. K. Rao, and M. D. Poliks, “A STATE-OF-THE-ART REVIEW ON AEROSOL JET PRINTING (AJP) ADDITIVE MANUFACTURING PROCESS,” 2019. [Online]. Available: http://asmedigitalcollection.asme.org/MSEC/proceedings-pdf/MSEC2019/58745/V001T01A035/6456423/v001t01a035-msec2019-3008.pdf.

[14] R. Al-Haidari *et al.*, “Planar SiC Power Module Packaging and Interconnections Using Direct Ink Writing,” in *2023 IEEE 73rd Electronic Components and Technology Conference (ECTC)*, May 2023, pp. 668–675, doi: 10.1109/ECTC51909.2023.00117.

[15] H. T. Friis, “A Note on a Simple Transmission Formula,” *Proc. IRE*, vol. 34, no. 5, pp. 254–256, May 1946, doi: 10.1109/JRPROC.1946.234568.

[16] A. S. Obeidat *et al.*, “Performance Evaluation of RF Novel Microstrip Lines Printed on Flexible Substrates,” in *2023 IEEE 73rd Electronic Components and Technology Conference (ECTC)*, May 2023, pp. 1471–1477, doi: 10.1109/ECTC51909.2023.00250.

[17] E. Enakerakpo *et al.*, “Passive UHF-RFID Tag With Printed Security Features for Authentication and Tamper Resistance,” *IEEE J. Radio Freq. Identif.*, vol. 8, pp. 49–57, 2024, doi: 10.1109/JRFID.2024.3382505.